Potential and current distribution across different layers of reinforcement in reinforced concrete cathodic protection system- A numerical study

Goyal, A., Olorunnipa, E. K., Sadeghi Pouya, H., Ganjian, E. & Olubanwo, A.

Original citation & hyperlink:
Goyal, A, Olorunnipa, EK, Sadeghi Pouya, H, Ganjian, E & Olubanwo, A 2020, 'Potential and current distribution across different layers of reinforcement in reinforced concrete cathodic protection system- A numerical study', Construction and Building Materials, vol. 262, 120580.
https://dx.doi.org/10.1016/j.conbuildmat.2020.120580

DOI 10.1016/j.conbuildmat.2020.120580
ISSN 0950-0618

Publisher: Elsevier

Potential and current distribution across different layers of reinforcement in reinforced concrete cathodic protection system- A numerical study

Arpit Goyal[1]

PhD scholar, Centre of Build and Natural Environment, Engineering, Environment, & Computing Building, Coventry University, Coventry, CV1 2JH, United Kingdom, Email: goyala4@uni.coventry.ac.uk, Orchid Id: 0000-0002-5016-6039

Ezekiel Kehinde Olorunnipa

MSc, Centre of Build and Natural Environment, Sir John Laing Building, Coventry University, Coventry, CV1 2HF, United Kingdom.

Homayoon Sadeghi Pouya

Assistant Professor, Centre of Build and Natural Environment, Engineering, Environment, & Computing Building, Coventry University, Coventry, CV1 2JH, United Kingdom.

Senior Materials Engineer, Structural Rehabilitation, Transportation UK and Europe, Atkins, Birmingham, United Kingdom,

Eshmaiel Ganjian

Professor, Centre of Build and Natural Environment, Engineering, Environment, & Computing Building, Coventry University, Coventry, CV1 2JH, United Kingdom.

Adegoke Omotayo Olubanwo

Assistant Professor, School of Energy, Construction and Environment, Sir John Laing Building, Coventry University, Coventry, CV1 2HF, United Kingdom.

Abstract

Cathodic Protection (CP) is being applied extensively to protect reinforced concrete structures exposed to aggressive environment from corrosion. However, protection provided by cathodic protection is dependent on several parameters such as concrete resistivity, applied current density and the geometrical arrangement of anode and cathode. For the first time, the distribution of potential and protection current along different layers of reinforcement in concrete is numerically investigated. A parametric study was done to analyse the effect of applied current density and concrete resistivity on protection achieved by different layers of reinforcement. The results show, concrete with anode applied at one surface is only able to protect top two reinforcement layers with current density of 40 mA/m^2, compared to anode at

[1] Corresponding author

two adjacent concrete surfaces which protect all four layers of reinforcement with minimum 10 mA/m^2 of current density. 80-90% of protection current reached the top layer of steel near the anode. Bottom layers of reinforcement received very minimal current and thus shows negligible protection. A drastic drop in protection was observed on moving down the reinforcement layers. Moreover, protection provided is highly depended on concrete resistivity.

Keywords: - Steel reinforced concrete; Polarization; Modelling; Cathodic Protection; Corrosion; Potential and current distribution, Impressed Current

1.0 Introduction

Cathodic protection (CP) is one of the most widely used and accepted technique to protect chloride induced corrosion in reinforced concrete [1,2]. CP is dependent on delivering enough uniform current to the reinforcement to protect it from corrosion [3–5]. However, the magnitude of protection achieved is dependent on a number of parameters and boundary conditions such as anode type, nature of the concrete component, concrete porosity, water and chloride content, concrete resistivity and geometrical arrangement [6–8]. Due to unusual geometrical arrangements of concrete and rebar such as areas of joints or with difficult access, it is hard to achieve uniform current distribution especially to the bottom reinforcement [9].

There has been limited research in the past to study the distribution of current and potential in reinforced concrete CP system. For modelling the ICCP system, different approaches have been reported in the literature viz. constant potential method, the constant current method, potential sweep and sheet resistance method. However, most of the literature is limited to constant potential and constant current methods only because of the simplification of the system. The other two methods have only been reported by Helm and Raupach in 2016 and 2019 [9,10]. Muehlenkamp et al. [11] studied the effect of moisture content on CP of steel in concrete by modelling thermally sprayed zinc as an anode. The authors observed that regardless

of the applied voltage or saturation level, back of the rebar received about 50% higher iron oxidation partial current density. Moreover, moisture significantly affects corrosion rate i.e. being more severe in dry conditions than wet conditions. Xu and Yao [12] studied the influence of initial corrosion rate and concrete resistivity on current distribution in reinforced concrete CP system with conductive mortar overlay anode through laboratory investigations. Hassanein et al. [13] analysed the effect of several parameters on the current distribution of CP through theoretical analysis and concluded that steel-concrete interface boundary conditions significantly affect current distribution.. In 2013, Cheung and Cao [14] conducted a numerical study to study the effect of macrocell corrosion on the current distribution in CP by modelling a slab geometry with upper corroding and lower passive bar. The authors observed that macrocell current exists for lower applied current densities and cathode protection current flows to passive rebar, even though geometry and resistivity favours the flow of current to top corroding bar. Bruns and Raupach [15] used potential sweep method to analyse the protection of the opposite reinforcement layer of RC structures by CP, considering zinc hydrogel as an ICCP anode. Polarization properties were applied in the model considering a linear relationship between anode current density and over-potential at the anode surface. The authors concluded that a very high protection current densities were required to achieve a 100 mV decay criterion for rear reinforcement. Moreover, in the case of lower concrete resistivity, polarization behaviour of the reinforcement mainly governs the current distribution between anode and cathode. Whereas, in the case of higher concrete resistivity, concrete resistance between anode and steel predominates CP current distribution [15].

All the above models reported by several authors are for various types of anodes. However, none of them have considered coating based anode system in the numerical modelling. However, in 2016, Helm and Raupach [9] presented a comparative study of all the modelling methods and proposing a sheet resistance method which considers both anode conductivity and

anode polarization behaviour. The authors applied all the approaches to a slab geometry with conductive organic coating anode applied on the surface and monitor potential and current distributions for different approaches of modelling. The results showed that the sheet resistance method is the best method to assess the realistic current and potential distribution in the anode/concrete interface and only method considering the voltage drop across the anode surface. In addition, author's mentioned that all the methods are suitable if the aim of the modelling is to get an approximate estimation of the polarization behaviour of the reinforcement [9]. However this model only works for highly conductive coating anode system. Later in 2018, they analysed the effect of various parameters on current and potential distribution for active and passive steel bars arrangement in a slab considering time-dependent analysis [10]. Other studies have been based on modelling corrosion of steel in concrete and to study the effect of macrocell corrosion [6,14,16].

It can be observed that anode properties and polarization behaviour have been neglected in all the methods except the sheet resistance method, which in turn has its own limitations. Moreover, except Helm and Raupach (2016) no one has considered conductive coating anode system. However, for conductive coating anodes, it is really important during designing stage to know the depth of the protection achieved to protect the lower depth reinforcement depending on type of elements and level of protection required. In addition, no one has looked at potential and current distribution along different layers of reinforcement in concrete. This will be useful to study the influence zone of anode, giving details of requirement of more anode placement.

The aim of this paper is to model current and potential distribution along different layers of reinforcement in reinforced concrete CP system for thin conductive coating anode system. The effects of different parameters such as concrete resistivity and applied anode current density have been studied through a parametric study. Furthermore, to validate the model, potential

distribution along different layers of rebar's in CP system has been studied for conductive coating anode system as per experimental investigations. The numerical analysis can give information about anode placement and required protection current and can be useful in designing and optimising an effective CP system.

2.0 Laboratory Experiments

To validate the numerical approach and to analyse potential and current distribution for multi-layer reinforcement, laboratory tests were carried out on beam specimens of dimension 500 x 350 x 120 mm (**Fig. 1a**). Concrete specimens were prepared as per BS 1881-125:2013 [17] to give 28 days compressive strength of 35 MPa. OPC cement was used at 360 kg/m^3. Fine and coarse aggregates of the maximum size of 4.75 mm and 20mm were used at 640 kg/m^3 and 1190 kg/m^3 respectively. The concrete mixes had a water to cement ratio of 0.5. 3% of NaCl by cement weight was added to the mix to accelerate corrosion of rebar in concrete and simulate structural elements subjected to road de-icing salts. All the specimens were cured in water with same chloride concentration as that of mix water for 28 days to ensure even chloride distribution. Thereafter, all the specimens were stored in controlled environment of 50 ± 5% relative humidity and a temperature of 20 ± 3 ^{o}C for 1 month before anode application.

Ribbed steel bars of 10 mm diameter were placed in 4 layers with a concrete cover of 25 mm and spacing of 100 mm all along the beam length (**Fig. 1b**). Zinc rich paint (ZRP) as the conductive coating was used as an anode material and applied at the top surface of concrete having dry film thickness of 300 μm. The anode properties have already been published by authors [4]. A total of 3 beams were cast and average result of them is presented.

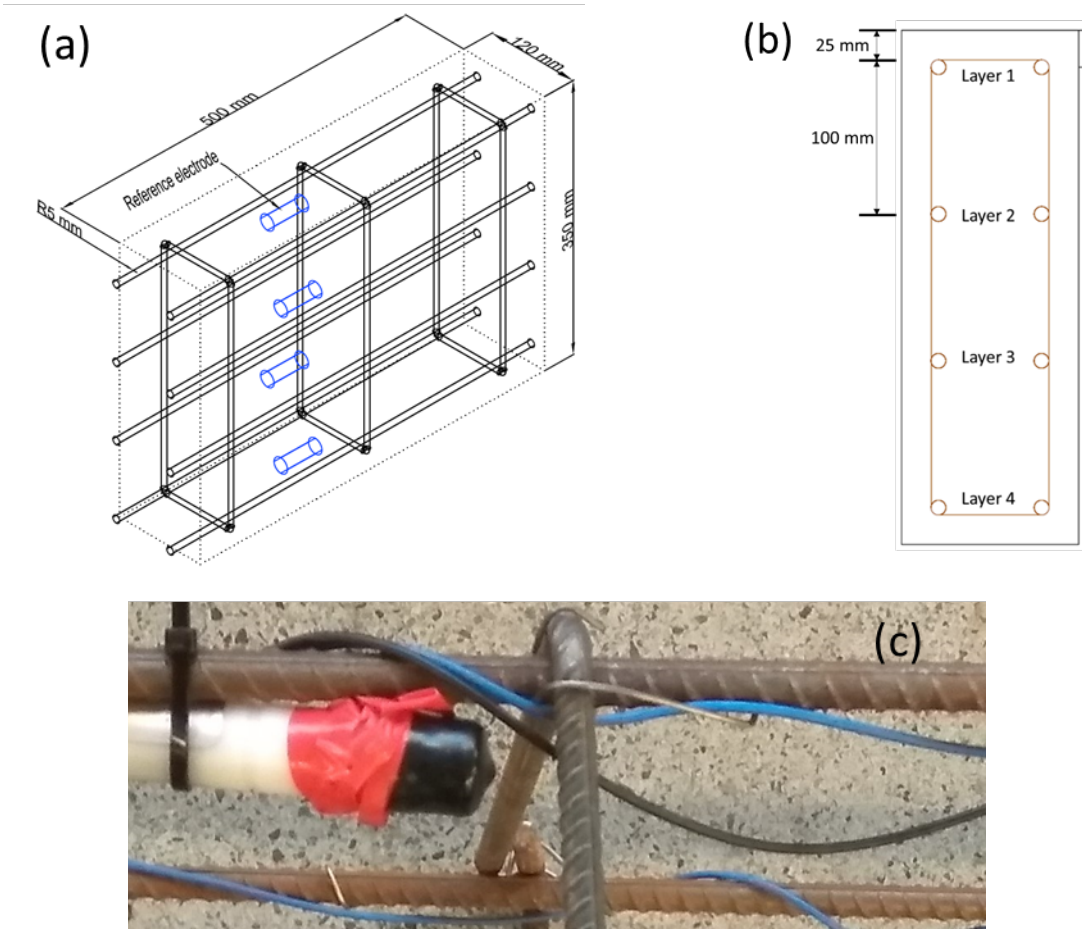

Fig. 1. (a) 3D Schematic of the beam specimen (b) Cross-section showing reinforcement layers (c) Reference electrode position with respect to steel bar

Experiments were carried out in an impressed current mode and the constant current density was applied between the anode and the steel bars. Each specimen was polarized for three different constant current densities i.e. 10, 20 and 40 mA/m^2 per steel surface area. Test was repeated three times on each beam for each current density to ensure repeatability of results. The Off-potential of the reinforcement bars were checked before polarizing which suggested steel to be in an active corrosion state.

For cathodically polarizing the specimen, steel bar was connected to the negative terminal and anode was connected to the positive terminal of the DC power supply. Potential distribution was monitored for a period of 4 days using silver-silver chloride (Ag/AgCl/0.5MKCl) reference

136 electrodes embedded in concrete at each reinforcement depth (**Fig. 1c**). A datalogger was used
137 to record the steel/concrete potential every minute for each steel depth, along with current
138 across the anode (Fig. 2). After this period, the depolarized potential was measured for 24 hrs.

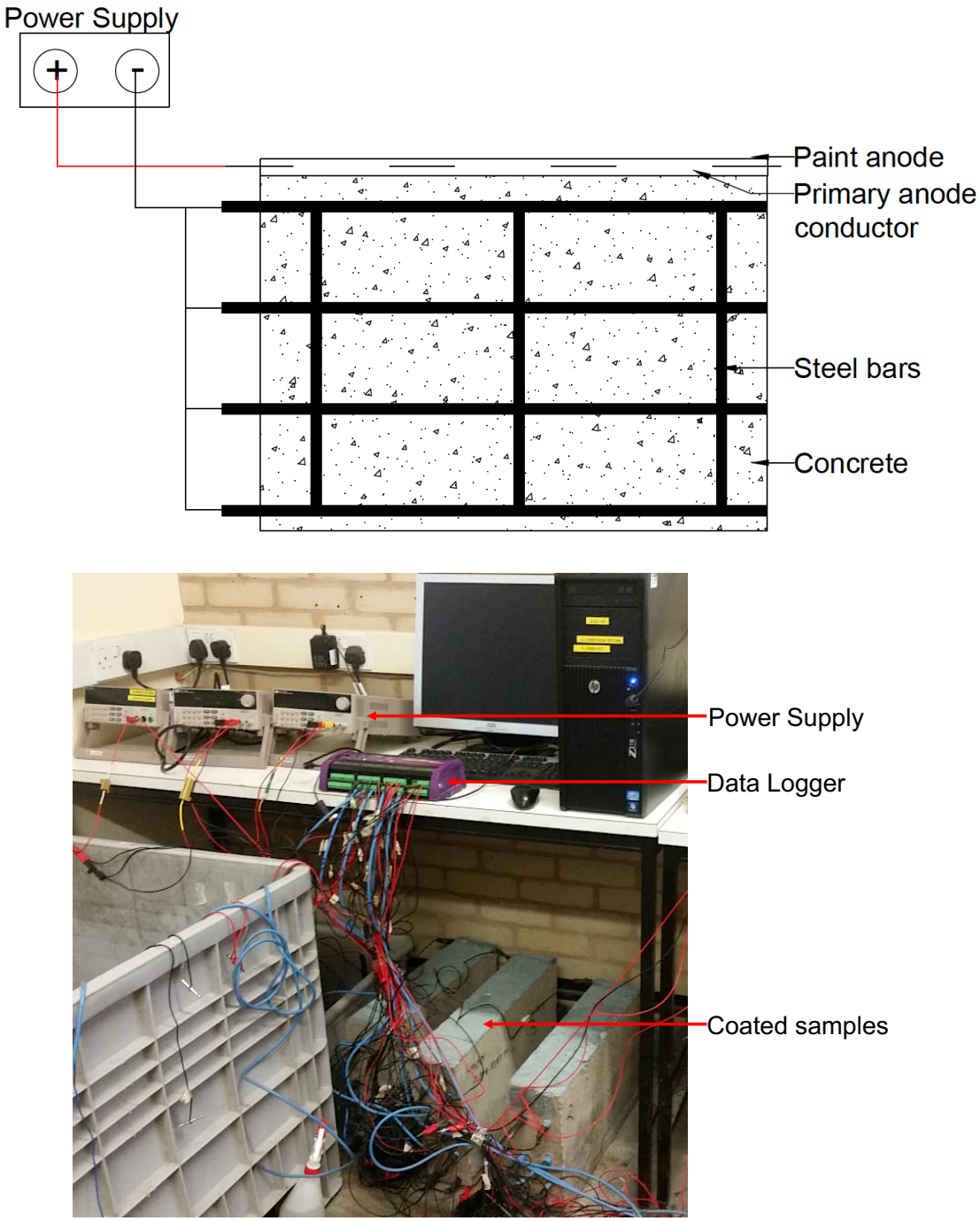

139 **Fig. 2.** Experimental setup and connections for cathodic polarization of the beam specimens

140

141

3.0 Numerical Model for CP analysis

3.1 General

The potential and current distribution inside the concrete follows Laplace equation (1) and Ohm's law (2), assuming electrolyte is homogeneous:

$$\nabla^2 E = 0 \qquad \text{(Equation 1)}$$

$$I_{xj} = \sigma \nabla E \qquad \text{(Equation 2)}$$

The total current density for any part of the electrolyte surface can be calculated using ohm's law as:

$$I_s = \sigma \frac{\partial E}{\partial n} \qquad \text{(Equation 3)}$$

Where ∇ is Nabla operator, ∇^2 is Laplace operator, I_{xj} (A) is current flowing in direction xj, E (V) is the difference between external electric potential of steel bar (considered as zero as a reference), I_s is total current density and electrolyte potential and σ (S/m) is the electrolyte conductivity of the concrete.

Two different electrode reactions were considered on the steel rebar boundary: iron oxidation and oxygen reduction:

$$Fe \rightarrow Fe^{2+} + 2e^- \qquad \text{(Equation 4)}$$

$$O_2 + H_2O + 4e^- \rightarrow 4OH^- \qquad \text{(Equation 5)}$$

Reaction kinetics of these reactions are modelled at the steel-concrete interface using the Tafel expressions obtained from polarization curves and fitting it into Butler Volmer Equation:

$$i = i^o\{\exp\left[\frac{2.303\eta}{b_a}\right] - \exp\left[\frac{-2.303\eta}{b_c}\right]\} \qquad \text{(Equation 6)}$$

Where i is current density on steel surface, i^o is exchange current density; b_a and b_c are anodic and cathodic Tafel slope and η is overpotential calculated for each reaction as:

$$\eta = E - E_{eq} \quad \text{(Equation 7)}$$

Where E_{eq} is equilibrium potential or free corrosion potential

At all isolating surfaces, vector normal to potential gradient is considered zero:

$$\frac{\partial E}{\partial n} = 0 \quad \text{(Equation 7)}$$

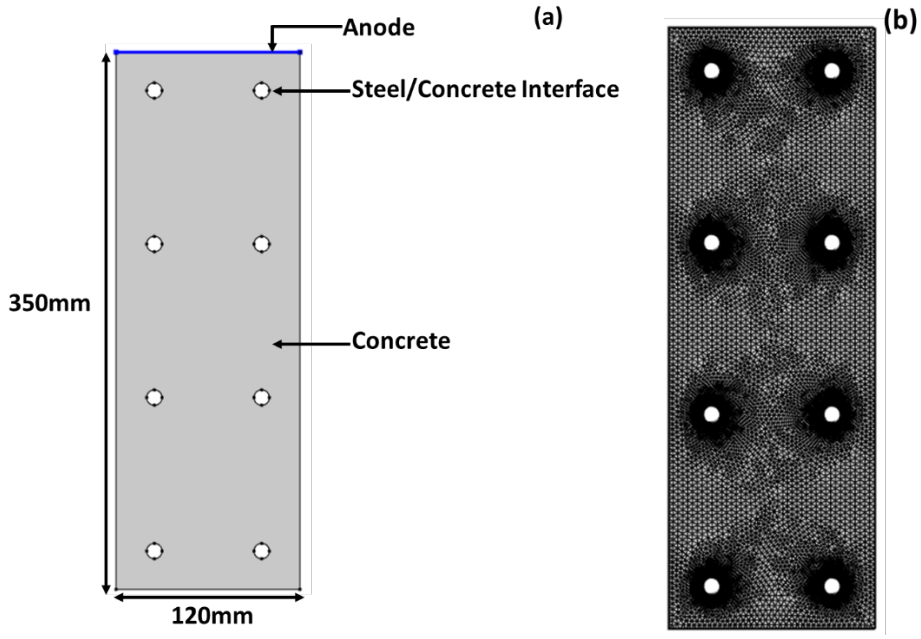

Fig. 3. (a) Model geometry (b) FEM mesh on the specimen geometry

The present simulation was carried out using finite element modelling software Comsol Multiphysics 5.3a in an impressed current mode. For this study, a similar geometry as of laboratory specimen and test have been modelled with the top surface of concrete considered as anode (**Fig. 3**). The mesh type used was triangular. A complete mesh consisted of 19992 elements with maximum and minimum element size of 3.5mm and 0.007mm, respectively, with a maximum growth rate of 1.1. Both anodic and cathodic reactions are considered at

steel/concrete interface. For the CP anode, a surface applied arrangement has been set and constant current density (I_{app}) was applied from top surface of concrete using electrolyte current density node as an inward electrolyte current density. The ZRP anode used for the present modelling is not highly conductive and falls in category of low conductive anode. The anode resistivity is almost of the same order of magnitude of concrete. As a consequence, the resistance of the anode, will play a negligible role in the problem if current is injected from the top as in sheet resistance method. Thus, constant current modelling method has been adopted for the modelling, which ignores anode resistivity and polarization behaviour. Moreover, all the reinforcement bars were considered to be in the active state. In order to ensure reliability of modelling, all initial conditions were obtained from experimental tests [18]. In numerical modelling, the IR drop cannot be considered. Thus, it was assumed that the final potentials obtained were instant-off potentials as considered in other studies [6,14,19,20]. Moreover, the difference between 'ON' and 'OFF' potentials was not significant and fairly uniform at different locations. Even incorporation of 'ON' potentials in the model will not change the conclusion.

3.2 Input Parameters and Parametric Study

For estimation of the polarization behaviour of steel, potentio-dynamic scans were carried out using a scan rate of 0.001V/sec. The results are shown in **Fig. 4**. Values obtained from the plot were fitted into equation 5 and used as initial parameters for the modelling as given in **Table 1**. Moreover, as chloride was mixed with water during casting, it is expected to have uniform corrosion throughout. The effect of chloride and moisture content is depicted in the equilibrium potential readings to represent the tested samples. In addition, electrical resistivity of concrete was required as input parameter and thus, measured using Wenner 4 probe method.

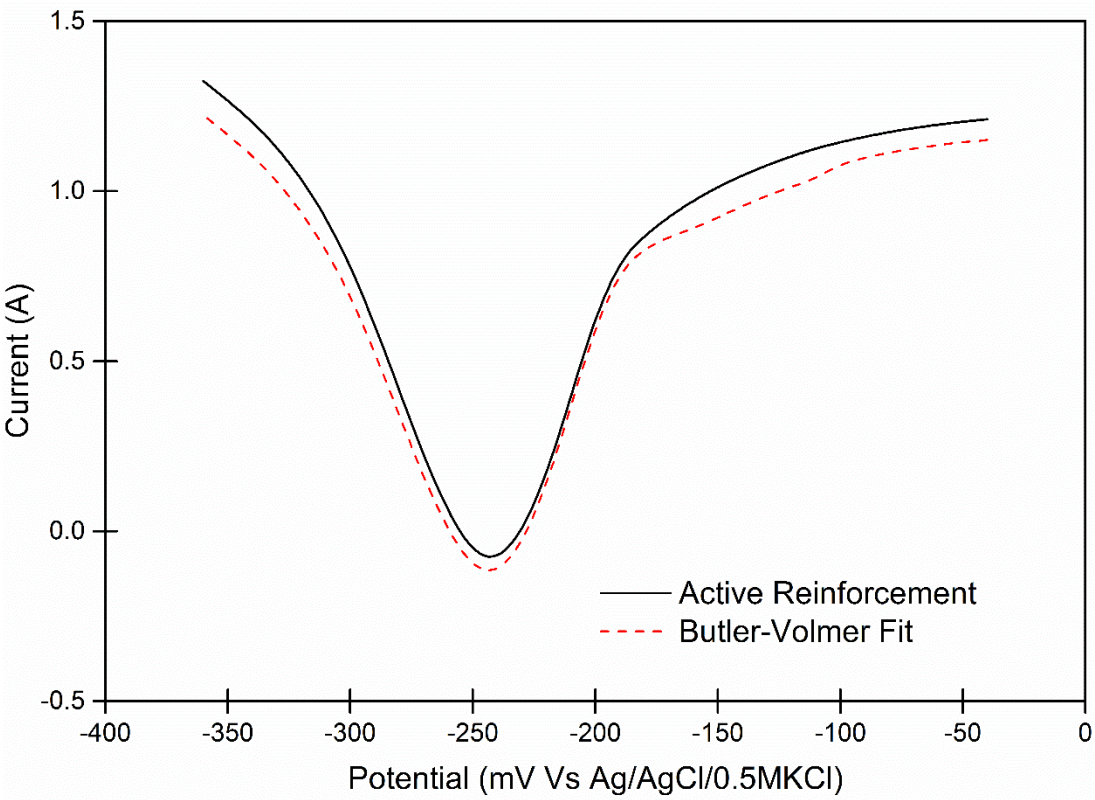

198 **Fig. 4.** Polarization curves for reinforcement

199 **Table 1** Fit parameters for conductive coating and active rebar

Parameter	Value
Equilibrium Potential, E_{eq} vs Ag/AgCl (V)	-0.245
Exchange Current Density, i^o (A/m^2)	1e-5
Anodic Tafel Slope, b_a (mV/dec)	22
Cathodic Tafel Slope, b_c (mV/dec)	-27
Concrete Resistivity (Ωm)	100

200 Further, to understand the influence of important parameters such as concrete resistivity and
201 applied current density, a parametric study was carried out. Bulk concrete resistivity was varied
202 from 100 Ωm to 500 Ωm reflecting water saturated condition and 2 kΩm to 10 kΩm reflecting
203 dry condition, as considered in the literature [6,9]. Applied current density was varied from 10
204 mA/m^2 to 20 mA/m^2, 30 mA/m^2 and 40 mA/m^2.

205

4.0 Result and Discussion

A comparison of the CP experiment and the numerical simulation of the specimen is shown in **Fig. 5.** The experimental values shown are instant off potentials measured at approximately 1s after turning off the power supply. **Fig. 5** shows good agreement between experimental and numerical results. The steel/concrete potential trend from both the methods was similar, however, the results obtained by two methods do not fully agree with each other. This phenomenon is attributed to experimental errors and simplification in FE such as neglecting anode properties and considering environmental conditions constant. Moreover, the experimental potential values are average result over certain space, however numerical simulation gives nodal values.

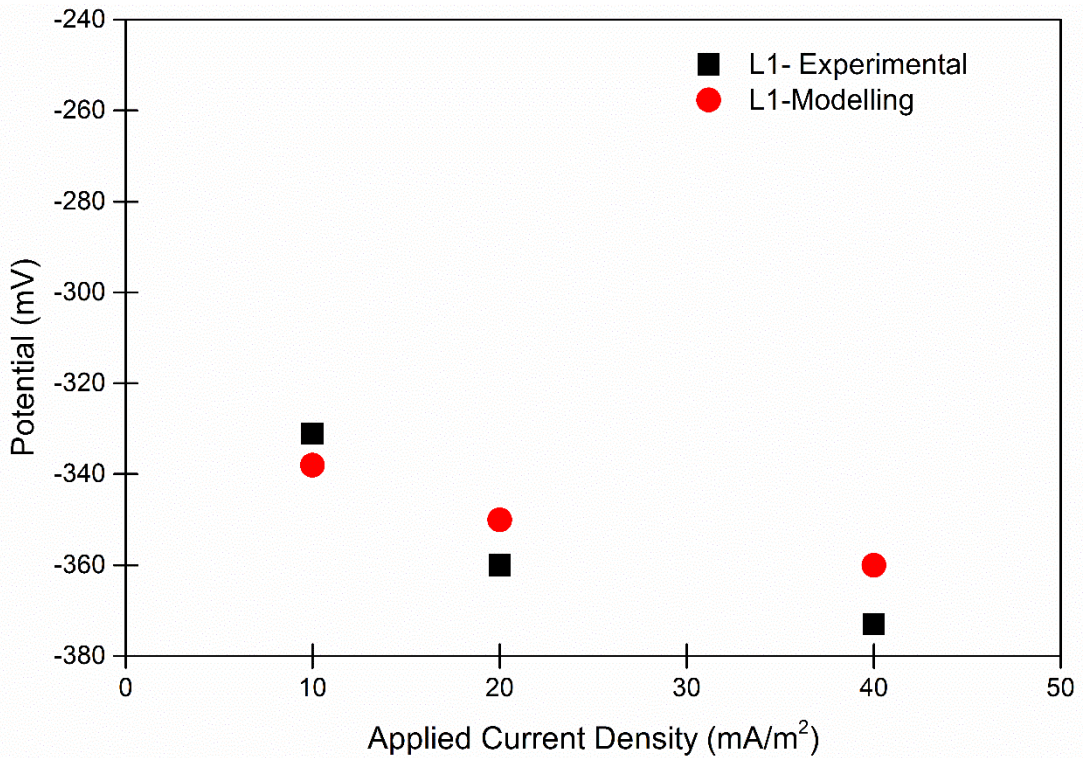

Fig. 5. Final Potential of layer 1 reinforcement at different applied current density measured experimentally and simulated numerically

4.1 Distribution of potential and current density in reinforcing steel with anode at the top surface

Fig. 6 shows the distribution of potential and current density in reinforcing steel and electrolyte potential for an applied anode current density of 10 mA/m^2 and concrete resistivity of 100Ωm, conditions similar to laboratory investigation. As observed, maximum current is received by the top bars nearest to the anode, thus showing the maximum potential shift. The potential and current reaching the steel decreases as moving farther away from the anode, as expected.

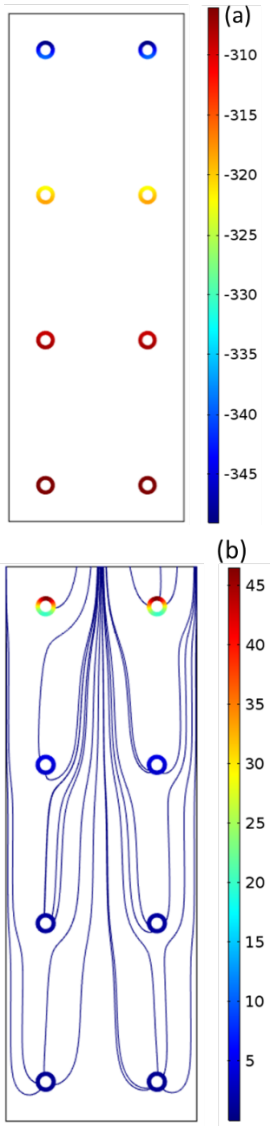

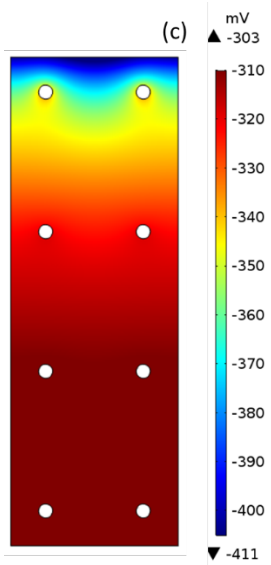

Fig. 6. Result of numerical simulation (a) Potential distribution of reinforcing steel (mV vs Ag/AgCl) (b) Current density distribution at reinforcing steel (mA/m^2) (c) Electrolyte potential distribution (mV vs Ag/AgCl) for anode at top surface

4.1.1 Parametric Study

Based on these results, the influence of a single parameter such as applied anode current density and concrete resistivity on potential and current distribution was analysed.

(a) Applied anode current density

Fig.s 7(a) and **7(b)** show the mean current density and the reinforcement potential shift at a point on top of the bar for all different layer of reinforcement respectively.

It can be observed that, even at an applied current density of 10 mA/m^2, potentials move towards more negative direction, indicating the effectiveness of cathodic protection. Nevertheless, as per BS 12696:2016, to satisfy CP protection criterion, at least 100 mV decay is required. This could be achieved if at least 100 mV potential shift is observed [21,22]. The numerical simulation result shows, about 20 mA/m^2 and 40 mA/m^2 anode current density is required to protect layer 1 and 2 of reinforcement respectively. However, in case of layer 3 and layer 4 of reinforcement, a current density significantly higher than 40 mA/m^2 would be

needed. It should be considered that the analysis has been carried out in steady state and the effect of long term protection is not incorporated in the numerical approach.

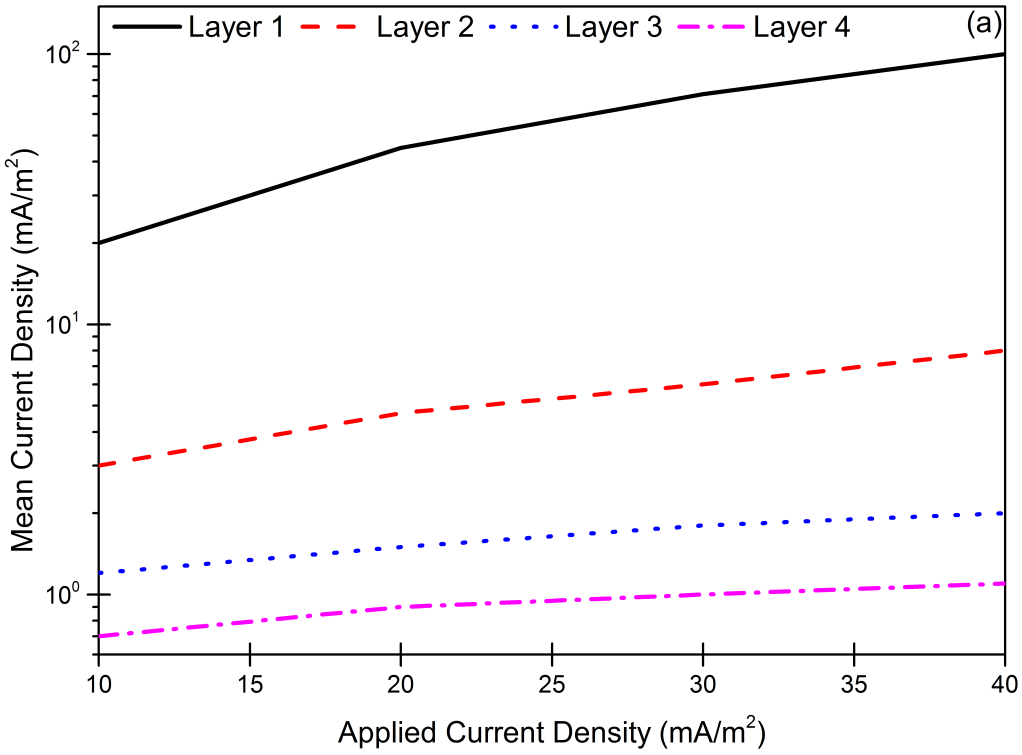

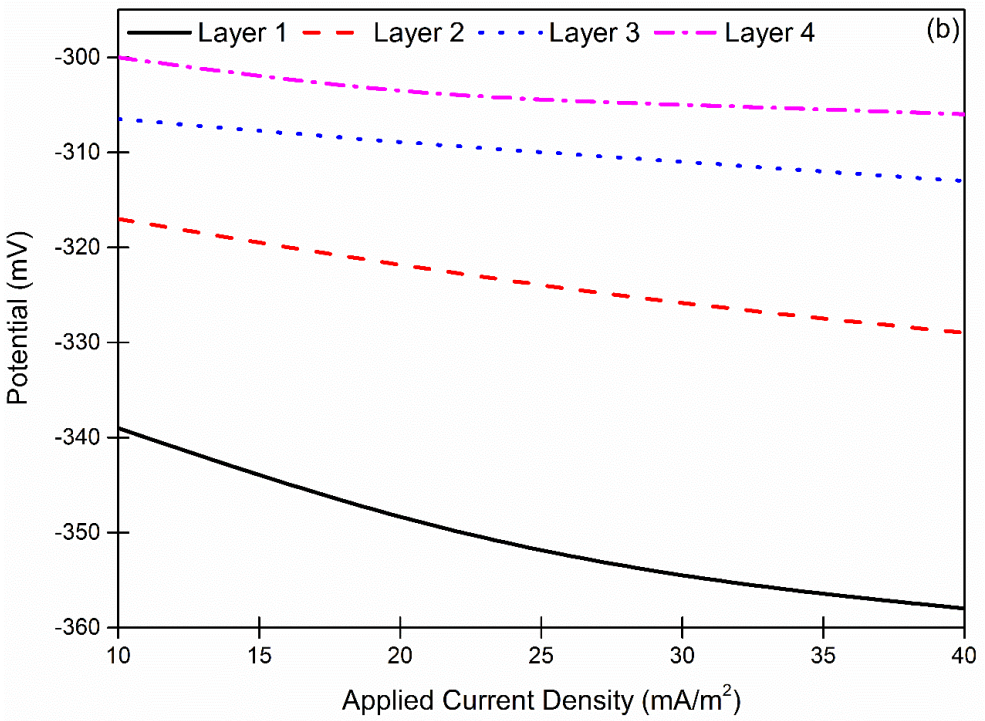

Fig. 7. (a) Mean current density (b) Potential at different layer of reinforcement relative to applied anode current density

The numerical simulation also shows a point to point current and potential values along the steel/concrete interface. **Fig. 8** shows potential distribution around steel-concrete interface under different applied current density for layer 1 and layer 4 of reinforcement. It can be clearly seen that a much higher protection current flows into the front (reverse arc length= 0mm) of the rebar surface facing the anode and have much larger potential shift compared to the back of the rebar (reverse arc length= 15.7mm). Moreover, potential difference between front to back decreases as we move from layer 1 to layer 4 of reinforcement. For Layer 1, the potential difference between front and back of the rebar for applied current density of 20 mA/m^2 was more than 10 mV, compared to layer 4, which shows less than 1 mV difference.

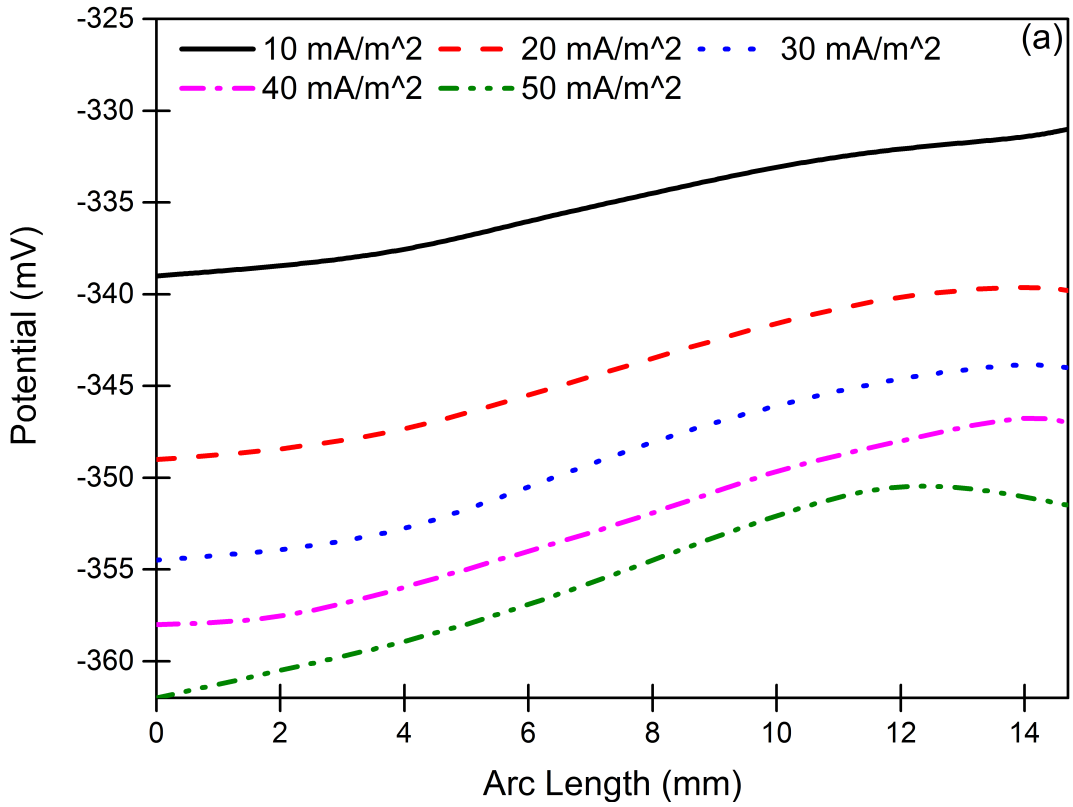

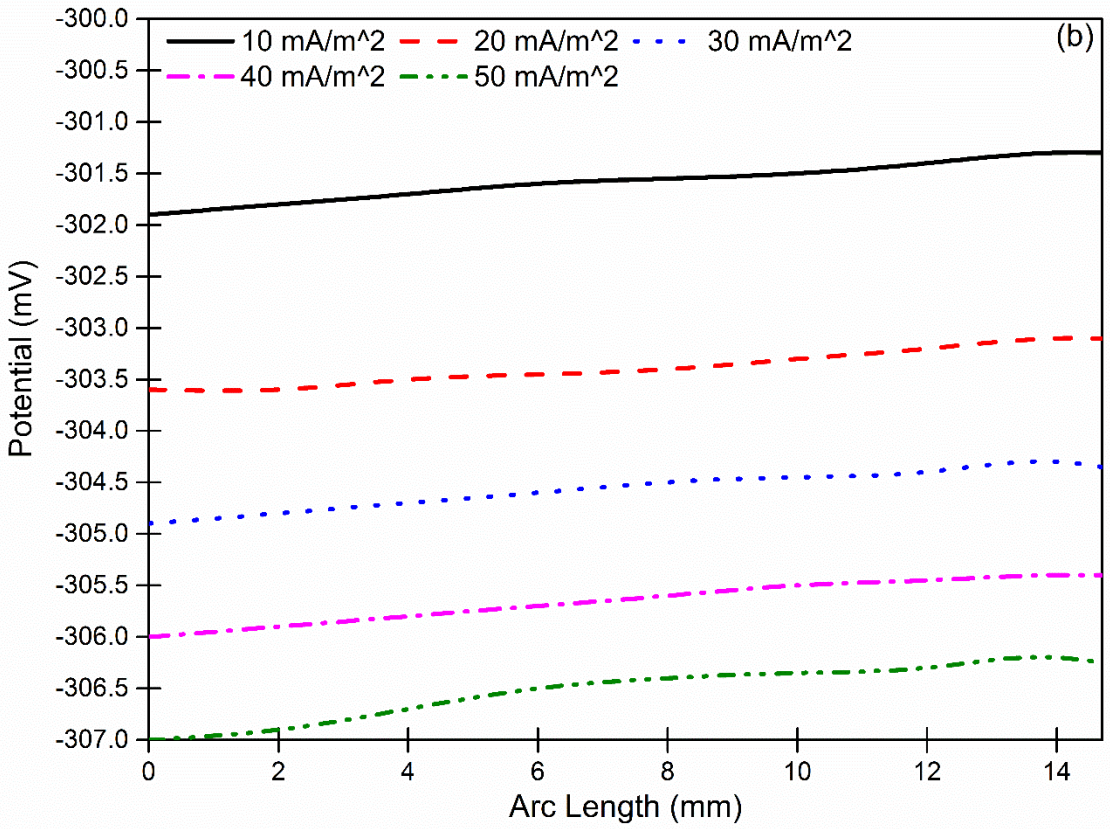

Fig. 8. Potential distribution around steel-concrete interface under different applied anode current density for (a) Layer 1 (b) Layer 4

Moreover, the fraction of total protection current density reaching different layer of reinforcement and the percentage current density received by each successive layer with respect to top layer at different applied anode current density is shown in **Table 2**. It can be observed that about 80-90% of the current density of the total protection current is reaching the top layer of reinforcement thereby showing a maximum potential shift. Remaining layer received less than 10% of the applied anode current density and this decreases with increase in the anode current density. There is drastic drop in the current received by the bottom layers, indicating the requirement of anode placement at more locations. To verify this, specimen with anode placed at two adjacent sides of concrete have been modelled and presented in next section.

Table 2 Fraction of total protection current density received by each successive layer for different current densities

Applied current density (mA/m^2)	Steel bar layer	Mean average current density (mA/m^2)	Percentage of total protection current density (%)	Percentage current density received as per layer above it (%)
10	Layer 1	19.8	80	-
	Layer 2	3.0	12	15
	Layer 3	1.2	05	06
	Layer 4	0.8	03	04
20	Layer 1	46.3	86	-
	Layer 2	4.7	09	10
	Layer 3	1.6	03	3.5
	Layer 4	0.9	02	02
40	Layer 1	103	90	-
	Layer 2	7.9	07	08
	Layer 3	2.0	02	02
	Layer 4	1.1	01	01

(b) Concrete Resistivity

Fig. 9(a) and **9(b)** show change in potential and current distribution with respect to change in concrete resistivity at an applied anode current density of 10 mA/m^2. Results show a strong influence of the concrete resistivity on the potential and current distribution. Higher potential shift and current density at steel/concrete interface are observed for lower concrete resistivity i.e. for saturated concrete, except layer 1 of reinforcement, indicating more uniform distribution.

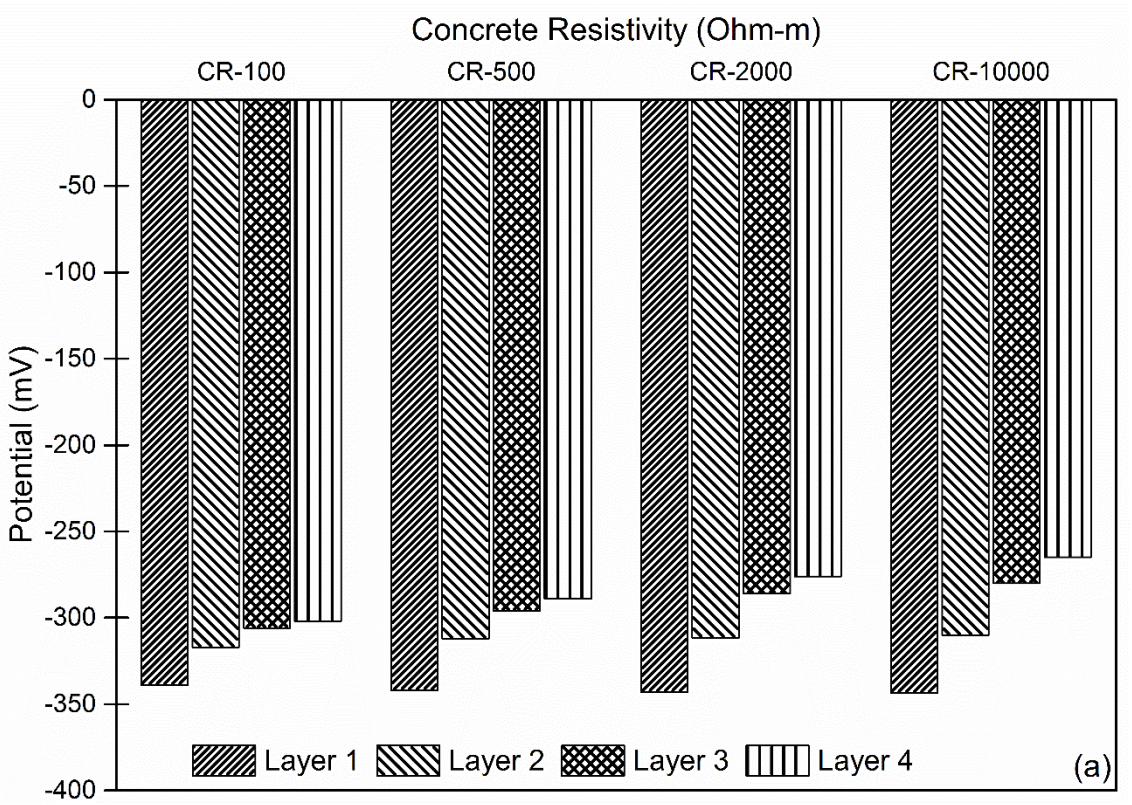

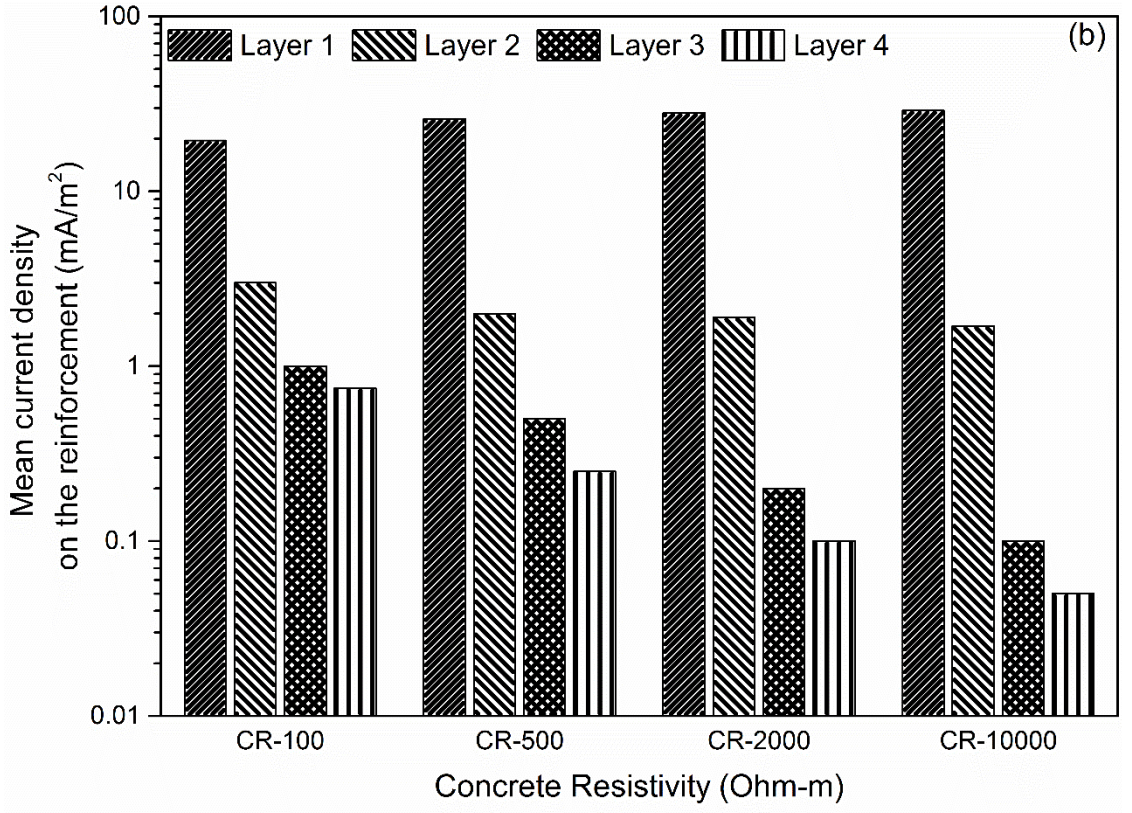

Fig. 9. (a) Potential (b) Mean current density on different layer of reinforcement relative to concrete resistivity

As concrete resistivity increases from 100 to 10000 Ωm, more current reaches the top layer compared to bottom layers for the same applied current density as high concrete resistivity prevents current to flow further down the concrete depth. By the time, current reached bottom layer, due to high resistivity it is negligible compared to Layer 1.

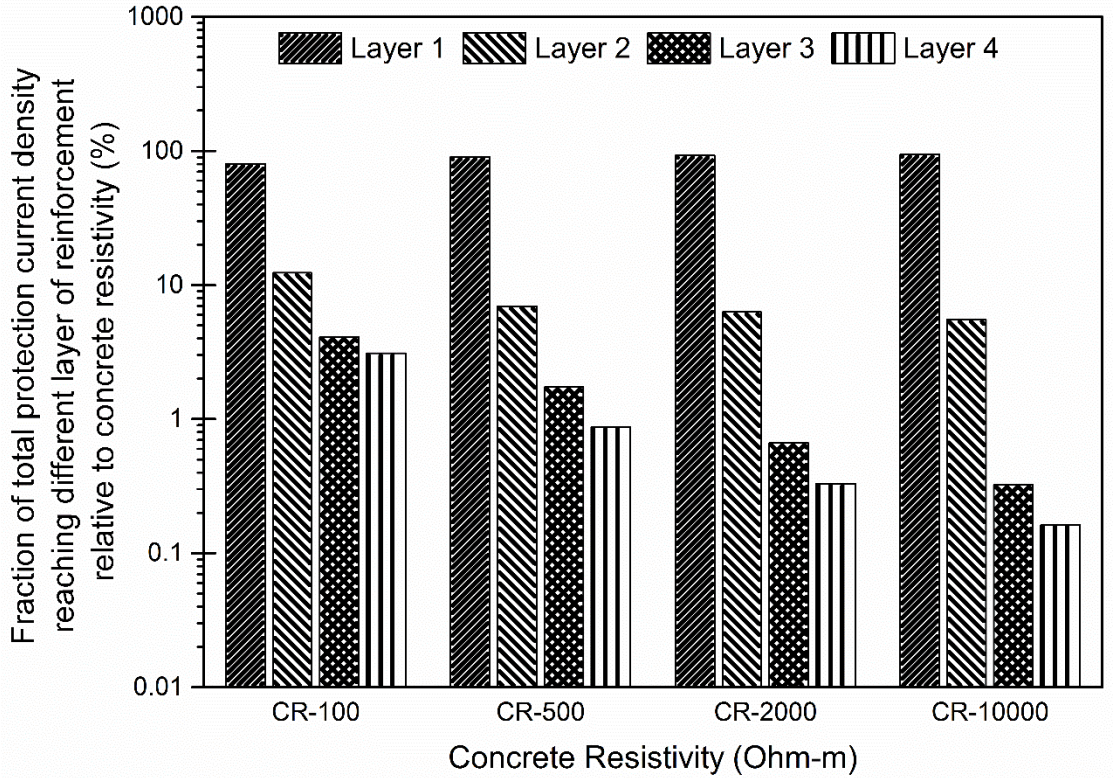

Fig. 10. Fraction of total protection current density reaching different layer of reinforcement relative to concrete resistivity

Fig. 10 shows a fraction of total protection current density reaching different layer of reinforcement for different concrete resistivity at an applied anode current density of 10 mA/m^2. It can be observed that the current is more uniformly distributed in case of saturated concrete. Also, as concrete resistivity increases, it was very difficult for current to reach bottom layers as we move away from anode. About 80-95% of total protection current reaches top face of layer 1 and this increases with increase in concrete resistivity. However, less than 10% of the protection current reaches other layers of reinforcement and this decreases with increase in concrete resistivity.

297 Hence, from the parametric study, it can be concluded that concrete resistivity and anode
298 current density has a strong influence on potential and current distribution.

299 **4.2 Distribution of potential and current density in reinforcing steel with anode at two**
300 **adjacent surfaces**

301 The above analysis showed requirement of anode distribution at more than only one face of
302 element to fully protect the bottom layers of reinforcement. For this case, a separate simulation
303 was carried out with anode placed at two adjacent concrete surfaces of the beam, as shown in
304 **Fig. 11**.

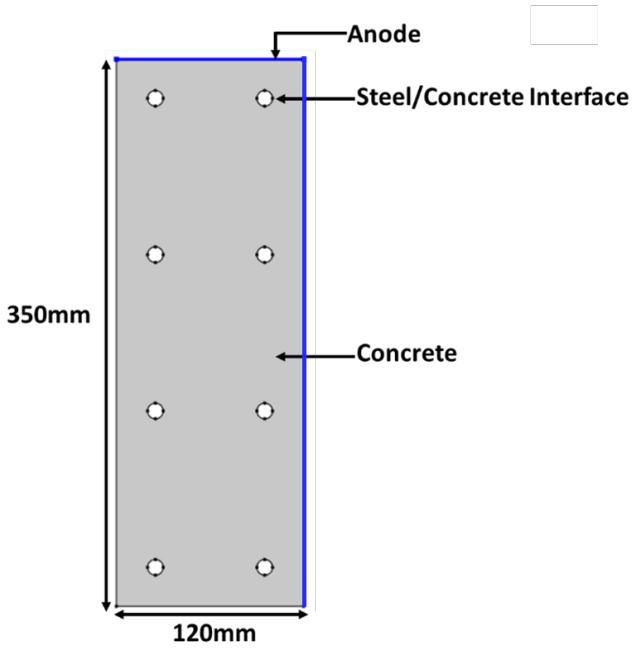

305 **Fig. 11.** Model geometry with anode placed at two adjacent sides

306 The potential shift for different layers of reinforcement is shown in **Fig. 12** and **Fig. 13**,
307 representing reinforcement immediately under the anode paint and away from it respectively.
308 It can be observed that all four layers of reinforcement, even at 10 mA/m^2 applied anode current
309 density show more than 100 mV potential shift, satisfying the criterion. This confirms that all
310 the reinforcement bars are fully protected. Moreover, reinforcement closer to the anode
311 receives more current and shows higher potential shift compared to rear reinforcement (**Fig.**

312 **14**). This confirms, that to fully protect the steel bars in this beam, anode is required to be
313 applied to two adjacent concrete surfaces.

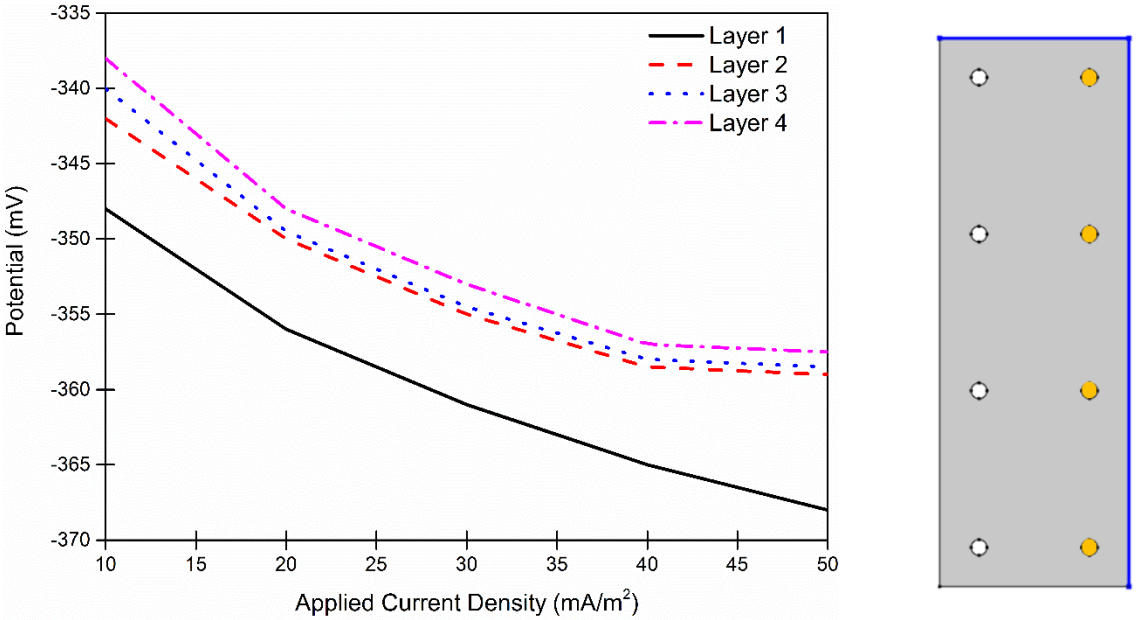

314 **Fig. 12.** Potential at different layer of reinforcement immediately under the anode relative to
315 anode current density

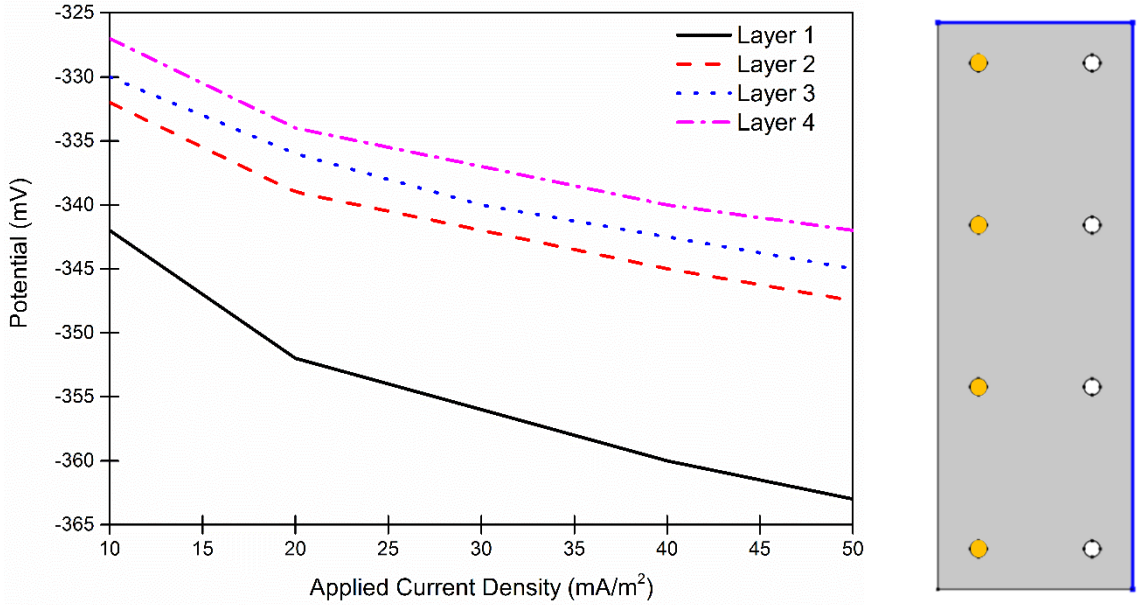

316 **Fig. 13.** Potential at different layer of reinforcement away from the anode relative to anode
317 current density

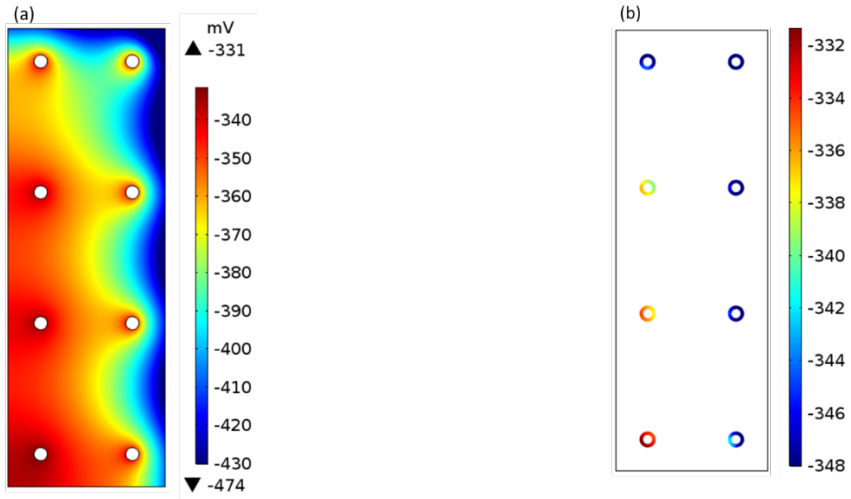

Fig. 14. (a) Electrolyte potential distribution (mV vs Ag/AgCl) (b) Potential distribution of reinforcing steel (mV vs Ag/AgCl) for anode at two adjacent sides

5.0 Conclusion

A numerical study was carried out to study the potential and current distribution across different layers of reinforcement of a cathodically protected element. The following conclusions can be drawn from the study:

1. The reinforcement layer closer to the anode receives maximum protection current and thus shows a maximum potential shift, compared to other reinforcement layers. This drastically decreases on moving away from the anode and therefore requires a very high protection current density to satisfy the 100mV decay criterion.
2. To protect lower layers of reinforcement, anode needs to have a more uniform distribution, preferably applied on sides of the beam. This is confirmed by a separate set of modelling with anode coated on two adjacent concrete surfaces. The result showed even anode current density of 10mA/m^2 can be sufficient to fully protect all the four layers of reinforcement from corrosion.
3. The parametric study showed a strong influence of concrete resistivity and applied anode current density on potential and current distribution. At low concrete resistivity between

reinforcement and anode, current distributes more uniformly, compared to higher concrete resistivity.

4. In practice, the factors such as bar size, number of stirrups and other geometrical arrangements will affect the potential and current distribution. Hence, numerical simulation can aid in designing an effective and economical CP system considering all the conditions which is difficult to estimate generally and results in under or over protection of the required protection current density. It can also be a useful tool to provide information about anode placement
5. Further analysis and model development is required considering time dependent analysis and anode polarization behaviour to study the effect of long term protection.

7.0 References

[1] A. Goyal, H. Sadeghi-Pouya, E. Ganjian, P. Claisse, A Review of Corrosion and Protection of Steel in Concrete, Arab. J. Sci. Eng. 43 (2018) 5035–5055. doi:10.1007/s13369-018-3303-2.

[2] L. Bertolini, E. Redaelli, Throwing power of cathodic prevention applied by means of sacrificial anodes to partially submerged marine reinforced concrete piles: Results of numerical simulations, Corros. Sci. 51 (2009) 2218–2230. doi:10.1016/j.corsci.2009.06.012.

[3] H. Sun, S. Ali, M. Yang, Degradation of carbon fiber reinforced polymer from cathodic protection process on exposure to NaOH and simulated pore water solutions, Mater. Struct. (2016). doi:10.1617/s11527-016-0859-8.

[4] A. Goyal, H.S. Pouya, E. Ganjian, Performance assessment of specialist conductive paint for cathodic protection of steel in reinforced concrete structures, Constr. Build. Mater. 223 (2019) 1083–1094.

359 [5] C. Andrade, Propagation of reinforcement corrosion : principles , testing and
360 modelling, Mater. Struct. 52 (2019) 2. doi:10.1617/s11527-018-1301-1.

361 [6] J. Warkus, M. Raupach, Modelling of reinforcement corrosion - geometrical effects on
362 macrocell corrosion, Mater. Corros. 61 (2010) 494–504.
363 doi:10.1002/maco.200905437.

364 [7] R. Montoya, W. Aperador, D.M. Bastidas, Influence of conductivity on cathodic
365 protection of reinforced alkali-activated slag mortar using the finite element method,
366 Corros. Sci. 51 (2009) 2857–2862. doi:10.1016/j.corsci.2009.08.020.

367 [8] H.M. Oleiwi, Y. Wang, M. Curioni, X. Chen, I. Shabalin, An experimental study of
368 cathodic protection for chloride contaminated reinforced concrete, Mater. Struct. 51
369 (2018) 1–11. doi:10.1617/s11527-018-1273-1.

370 [9] C. Helm, M. Raupach, Development of a numerical simulation model considering the
371 voltage drops within CP anode systems in RC structures, Mater. Corros. 67 (2016)
372 621–630. doi:10.1002/maco.201608832.

373 [10] C. Helm, M. Raupach, Numerical study on CP of RC structures regarding the
374 significance of the 100 mV decay criterion considering time dependent processes,
375 Mater. Corros. 70 (2019) 642–651. doi:10.1002/maco.201810486.

376 [11] E.B. Muehlenkamp, M.D. Koretsky, J.C. Westall, Effect of Moisture on the Spatial
377 Uniformity of Cathodic Protection of Steel in Reinforced Concrete, 61 (2005) 519–
378 533.

379 [12] J. Xu, W. Yao, Current distribution in reinforced concrete cathodic protection system
380 with conductive mortar overlay anode, Constr. Build. Mater. 23 (2009) 2220–2226.
381 doi:10.1016/j.conbuildmat.2008.12.002.

382 [13] A.M. Hassanein, G.K. Glass, N.R. Buenfeld, Protection current distribution in

reinforced concrete cathodic protection systems, Cem. Concr. Compos. 24 (2002) 159–167.

[14] M.M.S. Cheung, C. Cao, Application of cathodic protection for controlling macrocell corrosion in chloride contaminated RC structures, Constr. Build. Mater. 45 (2013) 199–207. doi:10.1016/j.conbuildmat.2013.04.010.

[15] M. Bruns, M. Raupach, Protection of the opposite reinforcement layer of RC-structures by CP - results of numerical simulations, Mater. Corros. 61 (2010) 505–511. doi:10.1002/maco.200905584.

[16] Y. Ji, W. Zhao, M. Zhou, H. Ma, P. Zeng, Corrosion current distribution of macrocell and microcell of steel bar in concrete exposed to chloride environments, Constr. Build. Mater. 47 (2013) 104–110. doi:10.1016/j.conbuildmat.2013.05.003.

[17] BSI, BS 1881 Part 125 : Methods for mixing and sampling fresh concrete in the laboratory, London, 2013. doi:Construction Standard, CS1:2010.

[18] L.Y. Xu, Y.F. Cheng, Experimental and numerical studies of effectiveness of cathodic protection at corrosion defects on pipelines, 78 (2014) 162–171. doi:10.1016/j.corsci.2013.09.011.

[19] R.B. Polder, W.H.A. Peelen, F. Lollini, E. Redaelli, L. Bertolini, Numerical design for cathodic protection systems for concrete, Mater. Corros. 60 (2009) 130–136. doi:10.1002/maco.200805056.

[20] M. Bruns, M. Raupach, C.P. Cp, CP of the rear reinforcement in RC-structures – Numerical modelling of the current distribution, (2009) 813–820.

[21] BSI, BS EN ISO 12696 Cathodic protection of steel in concrete, London, 2016.

[22] A. Goyal, H.S. Pouya, E. Ganjian, A.O. Olubanwo, M. Khorami, Predicting the

406 corrosion rate of steel in cathodically protected concrete using potential shift, Constr.
407 Build. Mater. 194 (2019). doi:10.1016/j.conbuildmat.2018.10.153.

408 **Declaration of Interest**

409 We wish to confirm that there are no known conflicts of interest associated with this publication
410 and there has been no significant financial support for this work that could have influenced its
411 outcome.